JPE 18-3-24

https://doi.org/10.6113/JPE.2018.18.3.902
ISSN(Print): 1598-2092 / ISSN(Online): 2093-4718

Investigation of Rise Time and Overshoot in Pulse Transformers with Different Topologies for Electromagnetic Trigger of SCRs

Gang Lv*, Dihui Zeng†, and Tong Zhou*

†,*School of Electrical Engineering, Beijing Jiaotong University, Beijing, China

Abstract

This study investigates the influences of different core parameters on the dynamic performances, such as rise time and overshoot, in pulse transformers for the triggering circuit of SCRs. First, a simplified transformer equivalent circuit, which emerges from a standard transformer equivalent circuit, is developed to analyze the step response. Second, the relations between the dynamic performances and the parasitic parameters are calculated by the simplified equivalent circuit. Third, the variations of rise time and overshoot, which are vital to the stability of triggering SCRs, with different core parameters, such as mechanic dimensions and topologies, are comprehensively investigated by analyzing the parasitic parameters. Finally, prototype transformers are fabricated to experimentally validate the analysis. The presented method can practically instruct the design of a pulse transformer for triggering SCRs.

Key words: Dynamic performance, Pulse transformer, Rectifier, Topology, Trigger circuit

I. INTRODUCTION

Pulse transformers are widely utilized in many fields, such as industrial high-power system and nuclear physics engineering. In the application of an industrial high-power converter, the isolation component, which is used to transmit the control signal to the high voltage side, is either the photoelectric or electromagnetic method. The photoelectric method is extensively applied in many apparatus; however, it is more complicated compared with the electromagnetic method [1]-[4] since the independent power supply must be set in each SCR block. Currently, the electromagnetic method is an optimal solution for this issue because of its cost, maintainability, and miniaturization.

The scheme of the electromagnetic method is shown in Fig. 1. The secondary side (high-voltage side) of the pulse transformer is connected to the gate of an SCR, and a pulse source, which is controlled by the logic circuit in the low-voltage side, is connected to the primary side of the transformer [5]. Then, the isolated triggering signal is transferred to the gate of the SCR through the transformer without any extra power supply.

The analyses of hysteresis and the accuracy of the current transformer, which is used to measure the component of the power system, are presented in [6]-[9]. Although the current transformer is more similar to the pulse transformer, these analyses are difficult to apply in analyzing the pulse transformer since they mainly focus on output accuracy and magnetic saturation. In [10]-[12], the secondary loads in the analysis are high-power klystrons or magnetrons. In these papers, the pulse transformers are mostly microsecond transformers, which apparently do not satisfy the requirement of the triggering SCR that needs a nanosecond one. Therefore, an analysis on the pulse transformer used in the electromagnetic trigger of SCRs is practically significant.

Since the dynamic performances of the pulse transformer are the key factors to SCR triggering, the present study first analyzes the requirements of a prototype SCR and its triggering pulse waveform. On the basis of the characteristics of stability in triggering SCRs [13], [14], the key parameters of the pulse transformer are determined from the requirements. A simplified equivalent circuit based on the standard equivalent circuit of the pulse transformer is analyzed. Then, an

Manuscript received Oct. 30, 2017; accepted Jan. 25, 2018
Recommended for publication by Associate Editor Yijie Wang.
†Corresponding Author: zengdh@bjtu.edu.cn
Tel: +86-105168-4100, Fax: +86-1051684100, Beijing Jiaotong Univ.
*School of Electrical Engineering, Beijing Jiaotong University, China

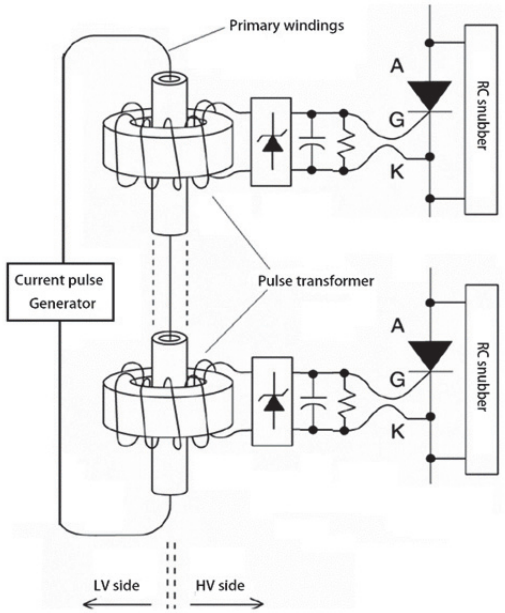

Fig. 1. Scheme of the electromagnetic trigger.

analytical method for predicting the parasitic parameters, which determine the dynamic performances, with various core parameters and topologies is proposed. Thus, this paper comprehensively discusses the influences of the core parameters and topologies on the dynamic performances, and relevant measurements are presented to validate the analysis.

II. Pulse Shape and Equivalent Circuits

In the applications of triggering SCR, the SCR turn-on depends on the amount of energy that can be safely dissipated in the region where switching is initiated, and a quasirectangular current pulse is demanded by the structural characteristics. A typical gate current pulse [15], [16] is shown in Fig. 2, and the gate current specifications for 5STP04D4200 are shown in Table I. According to the table, rise time and overshoot (peak current) are the crucial factors for triggering SCRs; specifically, dependable triggering means pulse energy is safely dissipated in a certain region. The experimental results presented by relevant papers indicate that only the overshoot (peak current) affects the magnitude of the anode current, *di/dt*. Although the rise time of the triggering pulse is insignificant for controlling anode current *di/dt*, it can lower the switching losses and improve the robustness of triggering.

In practice, obtaining an equivalent circuit for pulse transformers is a practical method for designing a prototype transformer. The waveform of the output current needs a quasi-rectangular curve. However, it contains a wide frequency spectrum. To transfer the current pulse with a minimum pulse distortion, especially during the rising stage, a maximum bandwidth is achieved, which means that the parasitic parameters should be minimized [17], [18].

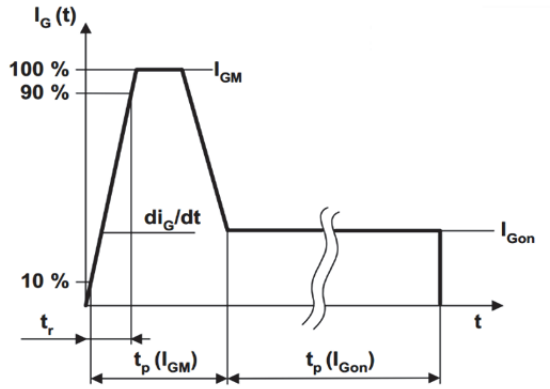

Fig. 2. Typical waveform of gating current pulse.

TABLE I
Specifications of Gating Current for 5STP04D4200

Quantity	Value
Peak forward gate current (I_{FGM})	10 A
Continuous pulse current (I_{Gon})	≤ 400 mA
Rate of gate current (di_g/dt)	≥ 2 A/μs
Width of gate pulse current (t_p)	5–20 μs

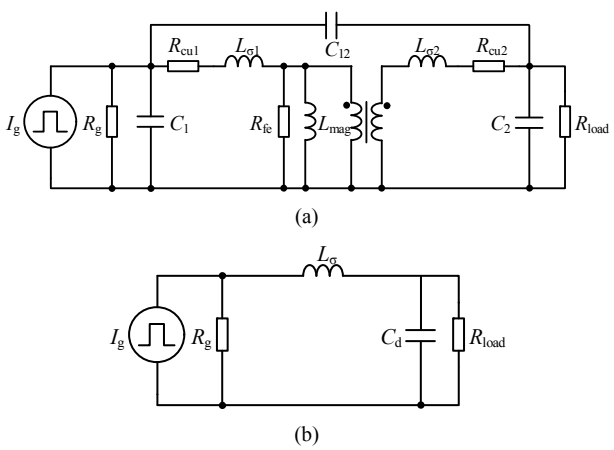

Fig. 3. Equivalent circuit of pulse CT. (a) IEEE standardized equivalent circuit. (b) Simplified equivalent circuit.

The IEEE standardized equivalent circuit of the pulse transformer is shown in Fig. 3(a) [19]. To simplify the analysis on the transient behavior with a quasi-rectangular current pulse, the standardized equivalent circuit can be simplified, as shown in Fig. 3(b). This simplified equivalent circuit can only be used for transient analysis during the rising edge if n>>1 [20]. Consequently, all impedances and the input source are transferred to the secondary, and the standardized transformer model can be ignored. In the following, all measured impedances are referred to the secondary if nothing mentioned. Since the pulse rise time T_r is within 100 ns and no excitation of the core occurs due to the small current-time-product, the influence of the core material (i.e. R_{fe} and L_{mag}) can be ignored during the rise

time. Even if the core resistance R_{fe} is considered, it is connected in parallel to the load resistance, which is R_{load} = 10 Ω in this case if it refers to the secondary or $R_{load,pri}$ = 1 mΩ if it refers to the primary and the turns ratio is set to 100. Similarly, the load resistance R_{load} is smaller than the resistance of the core material, which is R_{fe} ≈ 0.5 Ω on the primary.

According to the simplified circuit, rise time and overshoot are mainly affected by the leakage inductance L_σ and the equivalent capacitance C_d. During the rising stage, the transfer function of the simplified circuit is described as

$$F(s)=\left\{s\left[\frac{R_l L_\sigma C_d}{R_g}s^2+\left(\frac{L_\sigma}{R_g}+R_l C_d\right)s+\left(1+\frac{R_l}{R_g}\right)\right]\right\}^{-1}. \quad (1)$$

Assuming an ideal step current signal in the primary, the secondary output current i_{out} can be calculated with the inverse Laplace transform as follows:

$$i_{out}(t)=\frac{I_g R_g}{R_g+R_{load}}\left[1-e^{-at}\left(\frac{a}{k}\sinh(kt)+\cosh(kt)\right)\right] \quad (2)$$

with $k^2=a^2-b, 2a=\frac{R_g}{L_\sigma}+\frac{1}{C_d R_{load}}, b=\frac{1}{L_\sigma C_d}\left(1+\frac{R_g}{R_{load}}\right)$,

where the damping coefficient σ, which is extracted from (2), is defined as

$$\sigma=\frac{a}{\sqrt{b}}=\frac{C_d R_g R_{load}+L_\sigma}{2\sqrt{R_{load}L_\sigma C_d\left(R_g+R_{load}\right)}}. \quad (3)$$

As (3) describes, damping coefficient σ mainly depends on the internal resistance of the pulse source and the transformer characteristics. Even though a specific damping coefficient σ can be calculated by (3), its practicability is extremely limited when only the relation between the output pulse shape and the transformer characteristics is considered. Thus, the assumption is that the damping coefficient σ considers only the influence of the pulse transformer (the internal resistance of the pulse source is neglected), and (3) can be simplified to

$$\sigma=\frac{a}{\sqrt{b}}\approx\frac{1}{2R_{load}}\sqrt{\frac{L_\sigma}{C_d}}. \quad (4)$$

The normalized output current curves for the step transient response is shown in Fig. 4 at $T=\frac{\sqrt{b}}{2\pi}t$. The decreasing damping coefficient σ leads to faster rise time T_r. Starting from σ < 1, an overshoot is emerged. Therefore, to achieve a minimum rise time T_r, the damping coefficient σ should be minimal, while the resulting overshoot should be below the maximum gate current of the SCR. The overshoot may be calculated by

$$overshoot(\%)=1+e^{-a\pi/k}. \quad (5)$$

As (3) and (4) describe, the damping coefficient σ is determined by the parameters, such as leakage inductance L_σ, equivalent capacitance C_d, source internal resistance R_g, and load resistance R_{load}, which is a fixed value for a certain

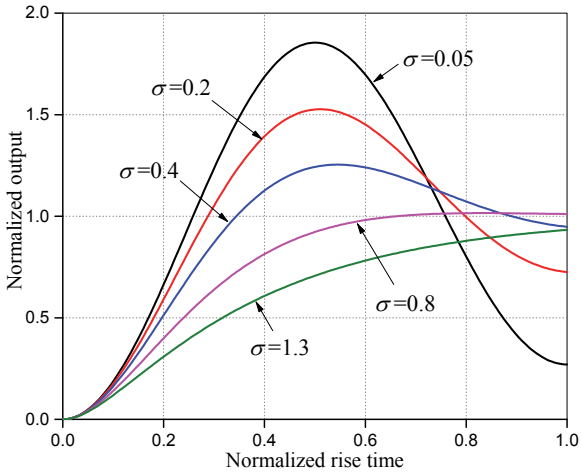

Fig. 4. Normalized rise time for step response.

type of SCR. Furthermore, the rated anode current directly determines the magnitude of the current pulse. In addition to the overshoot, the rise time T_r can be calculated by

$$T_r=\ln\left(-\frac{\sqrt{a-k}}{\sqrt{a+k}}\right)/k. \quad (6)$$

On the basis of (3) and (6), a small internal resistance and a high load resistance can achieve a fast rise time, a phenomenon that leads to an increase in rise time. Load resistance is normally a fixed value that cannot be adjusted. Thus, internal resistance, which is substantially related to the rise time with a fixed $L_\sigma C_d$-product, should be fully considered.

III. ANALYSIS

The dynamic performances of the transformer can be varied by its parasitic parameters. According to [20], the mechanical dimensions of a transformer directly determines the ratio of leakage inductance L_σ and equivalent capacitance C_d, which are the height and length of the winding, respectively. Moreover, the product of L_σ and C_d is defined by the transformer topology. In practice, it demands both the smallest $L_\sigma C_d$-product and the appropriate $L_\sigma C_d$-ratio to achieve the optimal dynamic performance of pulse transformation.

In the following, the three possible topologies for SCR triggering are comprehensively investigated, and the $L_\sigma C_d$-product of the three topologies is analyzed by electromagnetic energy theory, which can calculate leakage inductance L_σ and equivalent capacitance C_d with the energy stored in the electromagnetic field. They are described by (6) and (7), respectively [21–23].

$$E_{mag}=\frac{1}{2}\mu\int_V \vec{H}^2 dV=\frac{1}{2}L_\sigma I^2 \quad (6)$$

$$E_{elec}=\frac{1}{2}\varepsilon\int_V \vec{E}^2 dV=\frac{1}{2}C_d V^2 \quad (7)$$

where μ is the permeability of the magnetic core, ε is the permittivity of the gap between the bobbins, I_{pri} is the primary winding's current, V_{pri} is the primary winding's voltage, and dV is the volume element in the magnetic core. To simplify the comparison, only the energies between the windings are considered.

A. Toroidal Winding Type I

Toroidal winding topology (type I) is widely used in the triggering circuit of high-voltage apparatus in which the series SCR is needed due to its special construction Fig. 5(a) whose primary winding crosses the center of the transformer.

The leakage inductance L_σ and the equivalent capacitance C_d are defined by the mechanical dimensions of the transformer. For this topology [Fig. 5(b) and (c)], L_σ and C_d are analyzed as follows.

On the basis of Ampere's law and assuming an ideal magnetic core material ($\mu = \infty$), the magnetic field strength $|\vec{H}|$ can be described by (8):

$$|\vec{H}| = \frac{N_{pri}I}{2\pi R_m} \tag{8}$$

where N_{pri} is the turns of the primary winding, and R_m is the magnetic path radius of the core.

In [22], [23], the arithmetic average value is used as the equivalent value for magnetic field strength to simplify the calculation of inference. Magnetic field strength in the border of the core is described as

$$|H_i| = \frac{AI}{4\pi R_m}, \tag{9}$$

with $\mathrm{A} = \frac{1}{1-\frac{r_0}{R_m}} + \frac{1}{1+\frac{r_0}{R_m}}$.

The top and bottom of the stretched core are closed as shown in Fig. 5(c). Therefore, the integration path of magnetic strength is also closed. Assuming the current density J and the magnetic field strength $H(\rho)$ in the ribbons, then, the magnetomotive force is given by

$$\oint |H|dl = \int_0^{l_m} H(\rho)dl = H(\rho)l_m, \tag{10}$$

with

$$I_c = J(h-\rho)l_m,$$
$$\mathrm{H}(\rho) = H_i\left(1-\frac{\rho}{h}\right).$$

With Equations (10) and (6), the leakage inductance can be calculated by

$$L_{\sigma,toroidal} = \frac{\mu}{I^2}\int_0^h \left[H_i\left(1-\frac{\rho}{h}\right)\right]^2 2\pi l_m(\rho+r_0)d\rho$$
$$= \frac{A^2}{2}N_{pri}^2\pi\mu\frac{h}{l_m}\left(\frac{r_0}{3}+\frac{h}{12}\right). \tag{11}$$

According to the structure of the transformer bobbins, a linear voltage distribution is assumed across the windings. The distribution is defined by

$$V_{pri}(\theta) = V_{pri}; \qquad V_{sec}(\theta) = \frac{\theta}{2\pi}V_{sec} \tag{12}$$

where θ is the reference angle.

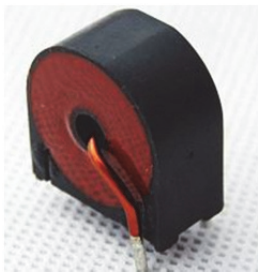

(a)

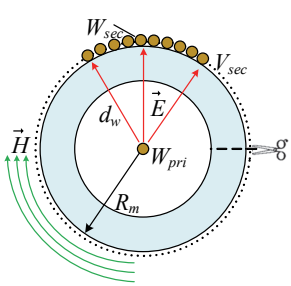

(b)

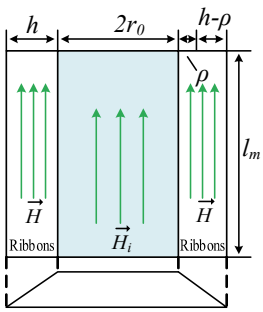

(c)

Fig. 5. Toroidal winding type I. (a) Real product. (b) Analysis model. (c) Stretched analysis model.

Therefore, the voltage difference between the primary and secondary winding depends on the angular position θ, i.e., $\Delta V(\theta) = V_{sec}(\theta) - V_{pri}(\theta)$. The electric field $E(\theta)$ depends on the θ-position, that is,

$$|E(\theta)| = \frac{\Delta V(\theta)}{r} = \frac{(n\theta-2\pi)}{2\pi r}V_{pri}. \tag{13}$$

With Equations (13) and (7), the relation between the equivalent capacitance and electric field energy is defined by

$$E_{elec} = \frac{1}{2}\varepsilon\int_0^{2r_0}\int_0^{2\pi}\int_{R_0}^{R_m}\left(\frac{(n\theta-2\pi)}{2\pi}V_{pri}\right)^2\frac{1}{r}dr\,d\theta\,dz$$
$$= 2\varepsilon V_{pri}^2 r_0\pi\left(\frac{1}{3}n^2-n+1\right)(\ln R_m - \ln R_0) = \frac{1}{2}C_d V_{pri}^2 \tag{14}$$

where n is the ratio of $\frac{N_{sec}}{N_{pri}}$, and r_0 is the cross radius for the primary conductor.

Then, the equivalent capacitance C_d is calculated by

$$C_{d,toroidal,i} = 4\varepsilon r_0\pi\left(\frac{1}{3}n^2-n+1\right)(\ln R_m - \ln R_0). \tag{15}$$

B. Toroidal Winding Type II

Given that the primary winding is limited to only one turn, the magnetic field strength excited by the primary cannot be improved with a limited primary current. Thus, this topology is no longer suitable for triggering the high anode current SCR. The type II topology, as shown in Fig. 6(a), obviously satisfies SCR needs. However, the primary winding of this topology is difficult to install due to the primary wounds on the bobbins, which are the same as those of the secondary winding. Therefore, this topology is used in the triggering circuit of a high-power apparatus.

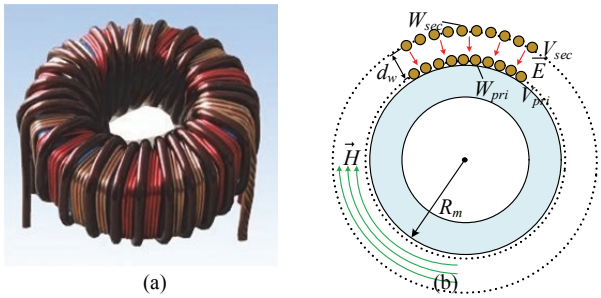

(a) (b)

Fig. 6. Toroidal winding type II. (a) Real product. (b) Analysis model.

In the following, the equivalent capacitance of this topology is mainly analyzed, as shown in Fig. 6 (b), because the analysis of the leakage inductance is the same as that of the toroidal winding type I. Then, a linear voltage distribution, the electric field $E(\theta)$, and the stored electric energy are described in (16) to (18), respectively.

$$V_{pri}(\theta) = \frac{\theta}{2\pi} V_{pri}; \qquad V_{sec}(\theta) = \frac{\theta}{2\pi} V_{sec} \tag{16}$$

$$|E(\theta)| = \frac{\Delta V(\theta)}{r} \approx \frac{n\theta}{2\pi r} V_{sec} \tag{17}$$

$$E_{elec} = \frac{1}{2}\varepsilon \int_0^{2r_0} \int_0^{2\pi} \int_{R_m - d_w/2}^{R_m + d_w/2} \left(\frac{n\theta}{2\pi} V_{sec}\right)^2 \frac{1}{r} dr\, d\theta\, dz =$$

$$\frac{2}{3}\varepsilon r_0 \pi n^2 V_{sec}^2 [ln(R_m + d_w/2) - ln(R_m - d_w/2)] = \frac{1}{2} C_d \cdot V_{pri}^2 \tag{18}$$

The equivalent capacitance C_d and the $L_\sigma C_d$-product of the transformer are then expressed as follows:

$$C_{d,toroidal,ii} = \frac{4}{3}\varepsilon r_0 \pi n^4 [ln(R_m + d_w/2) - ln(R_m - d_w/2)] \tag{19}$$

C. Parallel Winding

Another classical parallel winding topology that is widely used in many fields should also be considered. The primary and secondary winding are wound on two parallel bobbins, whose clearances are defined by their need for electrical insulation. For this topology Fig. 7(a), L_σ and C_d are analyzed as follows [21].

According to Ampere's law and assuming an ideal magnetic core material ($\mu = \infty$), the magnetic field strength $\vec{H}$ can be described by (20).

$$|\vec{H}| = \frac{N_{pri} I}{h_k} \tag{20}$$

where N_{pri} is the turns of the primary winding, and R_m is the magnetic path radius of the core.

With (20) and (6), the stored magnetic energy E_{mag} between the windings can be approximately calculated by (21), and l_w is the depth of the transformer core.

$$E_{mag} = \frac{1}{2}\mu (N_{pri} I)^2 \frac{l_w d_w}{h_k} = \frac{1}{2} L_\sigma I^2 \tag{21}$$

The leakage inductance $L_{\sigma,parallel}$ is

$$L_{\sigma,parallel} = \mu \frac{N_{pri}{}^2 l_w d_w}{h_k}. \tag{22}$$

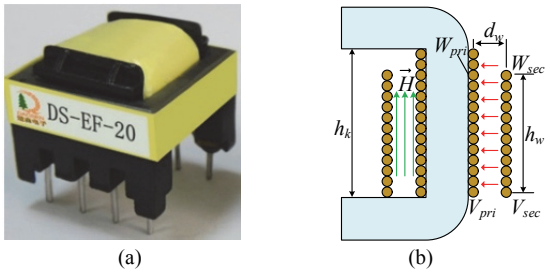

(a) (b)

Fig. 7. Parallel winding. (a) Real product. (b) Analysis model.

According to the bobbin structure of the transformer, a linear voltage distribution is assumed across the windings. The distribution is defined by

$$V_{pri}(y) = \frac{y}{h_w} V_{pri}; \qquad V_{sec}(y) = \frac{y}{h_w} V_{sec} \tag{23}$$

where y is the reference height.

Therefore, the voltage difference between the primary and secondary winding depends on the angular position θ, i.e., $\Delta V(y) = V_{sec}(y) - V_{pri}(y)$. The electric field $E(y)$ depends on the y-position, that is,

$$|E(y)| = \frac{\Delta V(y)}{d_w} = \frac{[V_{pri}(n-1)]y}{d_w h_w} \approx \frac{V_{sec} \cdot y}{d_w h_w}. \tag{24}$$

With Equations (24) and (7), the relation between the equivalent capacitance and the electric field energy is defined by

$$E_{elec} = \frac{1}{2}\varepsilon \int_0^{l_w} \int_0^{h_w} \int_0^{d_w} \left(\frac{V_{sec} \cdot y}{d_w h_w}\right)^2 dx\, dy\, dz$$
$$= \frac{1}{6}\varepsilon V_{sec}^2 \cdot \left(\frac{l_w h_w}{d_w}\right) = \frac{1}{2} C_d \cdot V_{pri}^2. \tag{25}$$

Then, the equivalent capacitance, C_d, is calculated by

$$C_{d,parallel} = \frac{1}{3}\varepsilon n^2 \left(\frac{l_w h_w}{d_w}\right). \tag{26}$$

D. Efficiency

The efficiency of the pulse transformer generally exceeds 95%. The losses in the transformer are negligible if only one transformer exists in the triggering circuit. However, the triggering circuit is equipped with several transformers (the specific number is dependent of the series of the SCRs). Therefore, the losses cannot be ignored in the analysis.

In this paper, the cross-section of the core is circular, while the primary and secondary winding resistances R_{cu1} and R_{cu2} are defined by

$$R_{cu1,2} = \frac{2\rho N_{1,2} \pi r_0}{S} \tag{27}$$

where ρ is the winding coil resistivity, S is the cross-section area of the winding coil, and $N_{1,2}$ is the turns of the primary or secondary winding.

Based on the handbook of the transformer, the equivalent resistance of the iron loss R_{fe} is given by

$$R_{fe} = C_{fe} f^{1.3} \left(\frac{\mu_1 N_{pri} I_m}{l}\right)^2 G \tag{28}$$

where C_{fe} is the coefficient to the core material, which can be obtained from the handbook; f is the supply frequency; G is the core weight; I_m is the magnetizing current; μ_1 is the core permeability; and l is the average length of the magnetic circuit.

In (27) and (28), the key component parameters in the equivalent circuit are proposed, and the total loss and efficiency in the transformer may be obtained.

E. Design Criteria

To calculate accurately, the parameters of the source and load should be considered. In practical applications, the pulse generator is connected to the primary side, and the load is connected to the secondary winding. Thereafter, a certain inductance L_{gen} or capacitance C_{load} occur and should be considered during the rise time and overshoot. In this design, the typical values of SCR are in the range of C_{load} = 100–1000 pF. Hence, Equation (4) should be extended to

$$\sigma = \frac{a}{\sqrt{b}} \approx \frac{1}{2R_{load}} \sqrt{\frac{L_\sigma + L_{gen}}{C_d + C_{load}}} . \quad (29)$$

IV. Simulations and Validations

The prototype transformers are fabricated, and each winding topology is used with various physical dimensions to test the object in the validation. The experimental circuit, as shown in Fig. 8, consists of a Schottky diode D_1, a 5STP04D4200 SCR D_2, and an ultra-low inductance resistor R_S. In the measurement, the voltage magnitude of R_S, which can be transferred to the current magnitude, is observed with an oscilloscope. The specifications of the instruments are presented in Table II.

The analytically predicted rise time, overshoot, and efficiency are provided in Figs. 9 to 12, and the main parameters of the prototype transformers are listed in Table III. The comparisons of the different values of the core cross-section radius or winding height are presented in these figures, which show the tendency of the dynamic performance with the variation of the core dimension or winding height.

In Fig. 9(a), the curves, which represent the different values of the core cross-section radius, rapidly decrease with the increasing core radius. This outcome basically conforms with the analytical results, since the reduction of the leakage inductance and the increase of the equivalent capacitance are augmented, while the core radius of the transformer increases. This phenomenon leads to a relatively shorter rise time. In Fig. 9(b), the curve trend is reversed since a short rise time causes a high overshoot, a trend that is consistent with Fig. 4. In Figs. 10 and 11, the curve trends are basically the same as in Fig. 9, and these analytical results are verified by measurements. In Fig. 12, the efficiency increases with the magnetic path length because the larger length will lower the flux density R_{fe}.

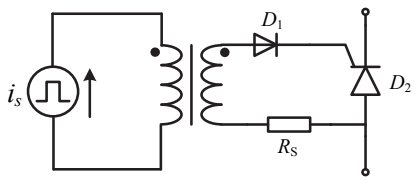

Fig. 8. Experimental circuit.

TABLE II
List of Experimental Equipment

Item	Type
Oscilloscope	GWINSTEK GDS-2102E
Signal generator	SUIN TFG1920B
DC supply	HUAWEI HD4825-2
Voltage probe	Tektronix TPP0201
Resistor	DALE 0.05R/5W
Oscilloscope	GWINSTEK GDS-2102E

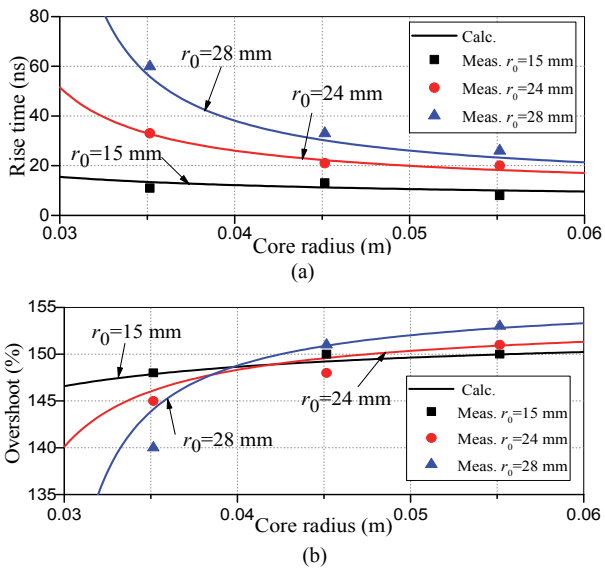

Fig. 9. Toroidal winding Type I. (a) Rise time. (b) Overshoot.

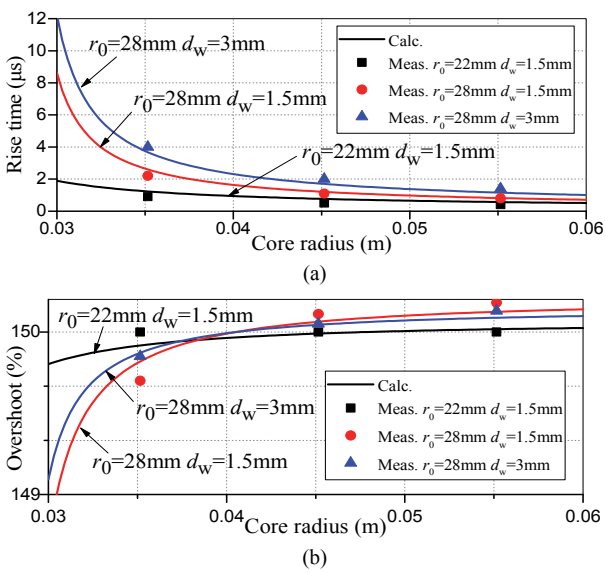

Fig. 10. Toroidal winding Type II. (a) Rise time. (b) Overshoot.

TABLE III
MAIN PARAMETERS OF PROTOTYPE TRANSFORMERS

Symbol	Quantity	Toroidal I	Toroidal II	Parallel	Unit
N	Turns ratio	200	200	200	
N_{pri}	Turns of primary	1	5	10	
N_{sec}	Turns of secondary	200	1000	2000	
r_0	Radius of core cross-section	15, 24, 28	22, 28	--	mm
d_w	Gap length between the primary and secondary winding	--	1.5, 3	5, 7, 10	mm
R_m	Radius of toroidal core	35, 45, 55	35, 45, 55	--	mm
h_w	Height of parallel winding core	--	--	32, 60, 87	mm
	Core materials	Si-Fe	Si-Fe	Si-Fe	
I_1	Rated pulse current	400	400	400	A
f	Rated pulse frequency	20	20	20	kHz

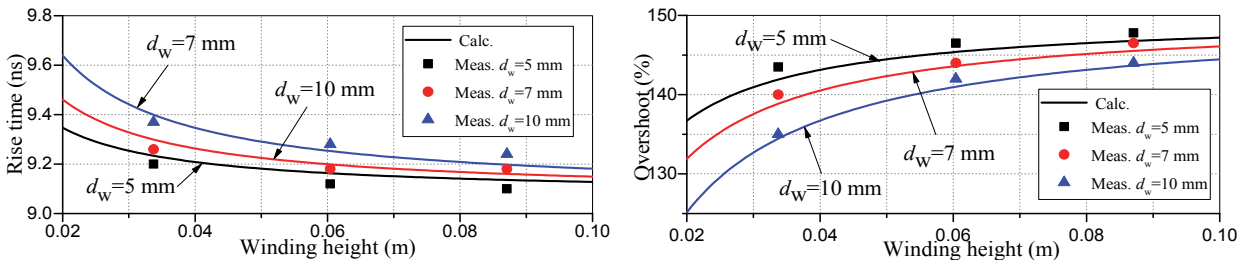

Fig. 11. Parallel winding. (a) Rise time. (b) Overshoot.

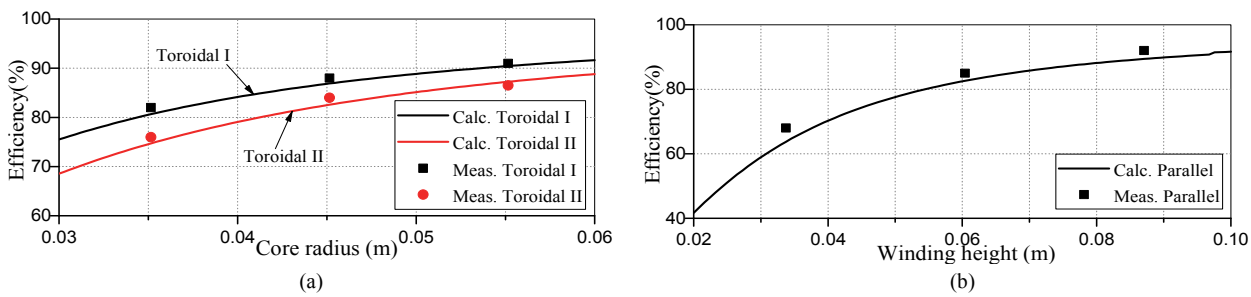

Fig. 12. Efficiency. (a) Toroidal winding I and II. (b) Parallel winding.

V. CONCLUSIONS

This paper briefly introduces the application of the triggering circuits of SCRs and the specifications of the triggering current pulse. According to this application, a simplified equivalent circuit is presented by extracting the standard equivalent circuit of the pulse transformer, which ignores the influence of some passive components that only affect the steady-state performance. The relation between dynamic performance, such as rise time and overshoot, and parasitic parameters is discussed by the analytical method. Furthermore, this investigation can aid in the design of the pulse transformer, improve the performance for triggering SCRs, and lower manufacturing cost.

ACKNOWLEDGMENT

This work was fully supported by the National Natural Science Foundation of China through Project Nos. 51377009 and 51777009.

REFERENCES

[1] D. M. Raonic, "SCR self-supplied gate driver for medium-voltage application with capacitor as storage element," *IEEE Trans. Ind. Electron.*, Vol. 36, No. 1, pp. 212-216, Jan. 2000.
[2] M. J. Johanson-Brown, "Thyristor Trigger Circuits," U.S. Patent 3502910, Mar. 24, 1970.
[3] D. E. Piccone, I. Somos, "Thyristor Turn-ON Circuits,"

U.S. Patent 3713101, Jan. 23, 1973.
[4] N. Hylten-Cavallius, C. I. Boksjo, and S. E. Lindblad, "Firing Circuit for Series-Connected Controlled Semiconductor Rectifiers," U.S. Patent 3593038, Aug. 13, 1965.
[5] X. Xie, J. Liu, F. Poon, and M. Pong, "A novel high frequency current-driven synchronous rectifier applicable to most switching topologies," *IEEE Trans. Power Electron.*, Vol. 16, No. 5, pp. 635-647, Sep. 2001.
[6] A. Wiszniewski, W. Rebizant, and L. Schiel, "Correction of current transformer transient performance," *IEEE Trans. Power Del.*, Vol. 23, No. 2, pp. 624-632, Apr. 2008.
[7] Rezaei-Zare, R. Iravani, M. Sanaye-Pasand, H. Mohseni, and S. Fahangi, "An accurate current transformer model based on preisach theory for the analysis of electromagnetic transients," *IEEE Trans. Power Del.*, Vol. 23, No. 1, pp. 233-242, Jan. 2008.
[8] U. D. Annakkage, P. G. Mclaren, E. Dirks, R. P. Jayasinghe, and A. D. Parker, "A current transformer model based on the Jiles-Atherton theory of ferromagnetic hysteresis," *IEEE Trans. Power Del.*, Vol. 15, No. 1, pp. 57-61, Jan. 2000.
[9] F. C. Guerra and W. S. Mota, "Current transformer model," *IEEE Trans. Power Del.*, Vol. 22, No. 1, pp. 187-194, Jan. 2007.
[10] J. Biela, D. Bortis, and J. W. Kolar, "Analytical modeling of pulse transformers for power modulators," in *IEEE 27th IPMS*, pp. 135-140, 2006.
[11] J. S. Oh, M. H. Cho, W. Namkung, K. H. Chung, T. Shintake, and H. Matsumoto, "Rise time analysis of pulsed klystron-modulator for efficiency improvement of linear colliders," *Nuclear Instruments and Methods in Physics Research section A*, Vol. 443, No. 2-3, pp. 223-230, Apr. 2000.
[12] D. Bortis, J. Biela, and J.W. Kolar, "Transient behavior of solid-state modulator with split core transformer," in *IEEE PPC*, pp. 1396-1401, 2009.
[13] L. Hudgins and W. M. Portnoy, "Gating effects on thyristor anode current di/dt," *IEEE Trans. Power Electron.*, Vol. 2, No. 2, pp. 149-153, Apr. 1987.
[14] K. Peter, W. Rik, and D. Doncker, "'Optimized gate drivers for internally commutated thyristors," *IEEE Trans. Ind. Electron.*, Vol. 45, No. 2, pp. 836-842, Mar. 2009.
[15] B. Kim, C. K. Kwang, and H. Eiki, "Study of switching characteristics of static induction thyristor for pulsed power applications," *IEEE Trans. Plasma Sci.*, Vol. 39, No. 3, pp. 901-905, Jan. 2011.
[16] Gate-drive Recommendations for Phase Control and Bi-Directionally Controlled Thyristors, ABB Switzerland Ltd., Switzerland, 2013.
[17] T. H. O'dell, "Design of a pulse-current transformer," *Electron. Lett.*, Vol. 16, No. 5, pp. 369-370, Aug. 1969.
[18] H. W. Lord, "Pulse Transformers," *IEEE Trans. Magn.*, Vol. 7, No. 1, pp. 17-28, Mar. 1971.
[19] IEEE Standards for Pulse Transformers, ANSI/IEEE Std. 390, 1987.
[20] MIT Radiation Laboratory, *Pulse Generators*, McGraw-Hill, 1948.
[21] D. Bortis, J. Biela, and G. Ortiz, "Design procedure for compact pulse transformers with rectangular pulse shape and fast rise times," *IEEE Trans. Dielectr. Electr. Insul.*, Vol. 18, No. 4, pp. 1171-1179, Aug. 2011.
[22] A. J. Binnie and T. R. Foord, "Leakage inductance and interwinding capacitance in toroidal ratio transformers," *IEEE Trans. Instrum. Meas.*, Vol. 26, No. 4, pp. 307-314, Dec. 1967.
[23] Hernandez, F. Leon, and P. Gomez, "Design formulas for the leakage inductance of toroidal distribution transformers," *IEEE Trans. Power Del.*, Vol. 26, No. 4, pp. 2197-2204, Jun. 2011.

Gang Lv received his Ph.D. degree in Electric Machine and Driven from Beijing Jiaotong University, Beijing, China, in 2007. From 2007 to 2009, he was a postdoctoral research fellow with the Technology Center, CRRC Qingdao Sifang Locomotive and Rolling Stock Co., Ltd., Qingdao, China. In 2007, he joined the School of Electrical Engineering, Beijing Jiaotong University, where he is currently an associate professor. His research interests include the application, control, and design of linear machines and drives and the analysis and control of ac traction machines.

Dihui Zeng received his M.Eng. degree in Mechatronic Engineering from China University of Mining and Technology, Beijing, China, in 2013. From 2013 to 2015, he was a Hardware Engineer with CRRC Zhuzhou Locomotive Institute Co., Ltd., Zhuzhou, China. He is currently working toward his Ph.D. degree in Electric Machine and Driven in Beijing Jiaotong University, China, where he has been engaged in linear motors.

Tong Zhou received his B.Eng. degree in Electrical Engineering from Qingdao University, Shandong, China, in 2013. He is currently working toward his Ph.D. degree in Electric Machine and Driven in Beijing Jiaotong University, China, where he has been engaged in the design and analysis of linear machines.